

Published in final edited form as:

ACS Appl Mater Interfaces. 2015 August 5; 7(30): 16395–16403. doi:10.1021/acsami.5b03532.

Enhancing the performances of P3HT:PCBM – MoS₃ based H₂-evolving photocathodes with interfacial layers

Tiphaine Bourgeteau¹, Denis Tondelier², Bernard Geffroy^{1,2}, Romain Brisse¹, Renaud Cornut¹, Vincent Artero³, and Bruno Jusselme^{1,*}

¹CEA Saclay, IRAMIS, NIMBE/UMR3685, Laboratory of Innovation in Surface Chemistry and Nanosciences (LICSEN), Gif-sur-Yvette, Cedex F-91191, France

²Laboratoire de Physique des Interfaces et Couches Minces (LPICM), CNRS UMR 7647, Ecole Polytechnique, Palaiseau, F-91128, France

³Laboratoire de Chimie et Biologie des Métaux, Université Grenoble Alpes, CNRS, CEA Life Science Division, 17 rue des Martyrs, F-38000, Grenoble, France

Abstract

Organic semiconductors have great potential for producing hydrogen in a durable and economically viable manner, as they rely on readily available materials and can be solution-processed over large areas. With the objective of building efficient hybrid organic-inorganic photo-electrochemical cells, we combined a noble metal-free and solution-processable catalyst for proton reduction, MoS₃, and a poly-(3-hexylthiophene):phenyl-C₆₁-butyric acid methyl ester (P3HT:PCBM) bulk heterojunction (BHJ). Different interfacial layers were investigated to improve the charge transfer between P3HT:PCBM and MoS₃. Metallic Al/Ti interfacial layers led to an increase of the photocurrent up to 8 mA cm⁻² at reversible hydrogen electrode (RHE) potential with a 0.6 V anodic shift of the HER onset potential, a value close to the open circuit potential of the P3HT:PCBM solar cell. A 50 nm thick C₆₀ layer also works as interfacial layer, with current density reaching 1 mA cm⁻² at RHE potential. Moreover, two recently highlighted¹ figures-of-merit, measuring the ratio of power saved, $\Phi_{\text{saved,ideal}}$ and $\Phi_{\text{saved,NPAC}}$, were evaluated and discussed to compare the performances of various photocathodes assessed in a three-electrode configuration. $\Phi_{\text{saved,ideal}}$ and $\Phi_{\text{saved,NPAC}}$ use the RHE and a non-photoactive electrode with identical catalyst as dark electrode, respectively. They provide different information especially for the differentiation of the role of the photogenerating layer and the role of the catalyst. Best results were obtained with the Al/Ti metallic interlayer, with $\Phi_{\text{saved,ideal}}$ and $\Phi_{\text{saved,NPAC}}$ reaching 0.64 % and 2.05 % respectively.

*Corresponding author: bruno.jusselme@cea.fr.

Associated content:

Supporting information available: Details of experimental procedures, supplementary Figures (Fig. S1 – S6) and STH efficiency and ratiometric power-saved figures-of-merit (Fig. S7 and S8). This material is available free of charge via the Internet at <http://pubs.acs.org>.

Keywords

organic photovoltaics; photocathode; hydrogen evolution reaction; organic semiconductor; photocatalysis; molybdenum sulfide

1. Introduction

Solar-to-chemical energy conversion is an attractive solution for the wide-scale storage and on-demand use of solar energy. Directly producing hydrogen from solar energy and water additionally participates in the building of a carbon-neutral economy. Though benchmarking with fossil resources based technologies is still challenging, the search for cost-effective and efficient photocatalytic systems is getting more and more important.

Photoelectrochemical (PEC) cells performing solar water splitting are widely reported in the literature, both in academic journals^{2,3} and in patents.⁴ They can have many different configurations depending on the absorber, catalysts and co-catalysts, number of photoelectrodes, buried junctions, etc.^{2,5} An ideal PEC device should meet several criteria:⁶ optical absorption in the IR-visible range (corresponding to 80 % of the solar flux), resistance to corrosion in aqueous electrolytes, solar-to-hydrogen conversion yield (STH) higher than 10 %, competitive cost on an energy-equivalent basis, absence of toxic effects, simple fabrication processes and great availability of materials.⁷ Performant devices exist, such as the AlGaAs/Si/RuO₂/Pt cell, reaching over 18 % of solar to chemical energy conversion.⁸ To reduce the cost linked to the use of expensive and rare materials, multi-junction silicon solar cells were used with earth-abundant catalysts by Rocheleau,⁹ Suzuki¹⁰ and Nocera,¹¹ reaching 7.8 % (wired configuration), 2.5 % (wireless configuration) and 4.7 % (wired configuration, 2.5 % in wireless configuration) respectively. Besides, cost-effective crystalline metal oxide semiconductors such as Cu₂O^{12,13} or BiVO₄^{14,15} have been used to build PEC cells other than the above-mentioned systems, with promising STH efficiencies.

Organic semiconductors (OSC) such as conducting polymers or fullerene derivatives are promising in the field of photovoltaic cells, which now display over 10 % power conversion efficiency (PCE)¹⁶ using abundant materials and low-cost processes. An advantage of using OSC in PEC is that thanks to chemical synthesis, a wide variety of materials can be obtained with different energy levels which can be tuned to the redox potentials required by water splitting catalysts to operate. OSC have thus been used for solar water splitting devices in different configurations. In a PV-electrolyzer configuration, an all-solution processed triple junction polymer solar cell with an open-circuit potential (V_{OC}) of 2.33 V was connected to an electrolyzer to perform water splitting.¹⁷ In a distinct approach, integrated photocathodes were built based on OSC such as polyaniline, polypyrrole, poly-(3-methylthiophene) or poly-(3-hexylthiophene) (P3HT), but only a few $\mu\text{A cm}^{-2}$ photocurrent were obtained in aqueous environment and the production of hydrogen was not always evidenced.¹⁸⁻²² Then, adding a fullerene acceptor to P3HT to form a P3HT:PCBM bulk heterojunction, this photocathode was used with NaCl as sacrificial donor, in a two electrode configuration and still without catalyst, and reached a peak current of 100 nA cm^{-2} .⁶ To enhance proton

reduction at the photocathode surface, a Pt catalyst was added at the top of an evaporated small molecule (phthalocyanine/fullerene) p/n planar junction and generated $800 \mu\text{A cm}^{-2}$ photocurrent corresponding to H_2 evolution from aqueous solution.²³ Recently, molybdenum sulfide (MoS_x) was used as both acceptor and catalyst in a nanocomposite polypyrrole-Ru/ MoS_x photocathode and delivered around $40 \mu\text{A cm}^{-2}$ at RHE potential.²⁴ In an earlier work, we studied a photocathode based on the photosensitization of a non-precious catalyst, MoS_3 , by a P3HT:PCBM bulk heterojunction (BHJ) in aqueous media.²⁵ MoS_3 was chosen as it is a noble metal-free hydrogen evolution catalyst (with an overpotential of 150 mV²⁶) and it can be solution-processed directly onto thin OSC films without thermal treatment, which could be detrimental to the organic layer. In this way, MoS_3 photo-produced hydrogen with a current density of $180 \mu\text{A cm}^{-2}$ at the reversible hydrogen electrode (RHE) potential. Another PEC cell based on P3HT:PCBM photocathode was recently reported to produce hydrogen from HCl-acidified acetonitrile solution with a cobaloxime catalyst, with 1 mA cm^{-2} photocurrent density.²⁷

In this work, we decided to investigate the possibility to enhance the performance in aqueous media of our system²⁵ through the introduction of a dense and conductive layer between the P3HT:PCBM layer and the MoS_3 catalyst. We report here on the results obtained with two different interfacial layers: (1) a metallic material used to improve electronic collection and electronic transfer to the catalyst, and (2) a nanocarbon layer used as fully organic interfacial layer. These two interfacial layers showed improved charge transfer compared to the initial cells without interfacial layers, as evidenced by the ratio of power saved under operation quantified through the determination of the ratiometric power-saved figures-of-merit $\Phi_{\text{saved,ideal}}$ and $\Phi_{\text{saved,NPAC}}$, as recently proposed par Lewis and coworkers.¹

2. Experimental

2.1. Chemicals and reagents

All manipulations were carried out under inert Ar atmosphere in a glovebox unless otherwise mentioned. PEDOT:PSS (AI 4083 for spin-coated devices) and P3HT (M104, RR = 96.3 %) were purchased from Ossila. PCBM was purchased from Solenn BV. ITO-coated glass substrates (XY20s) were purchased from Xinyan Technology Ltd. The MoS_3 nanoparticles suspension was prepared according to the literature²⁸ and a detailed procedure is given in the Supporting Information section.

2.2. Fabrication of the photocathodes

ITO/PEDOT:PSS/P3HT:PCBM—The P3HT:PCBM solution was prepared by dissolving 25 mg of P3HT and 25 mg of PCBM in 1 mL of anhydrous ortho-dichlorobenzene in the glovebox. The solution was stirred at 50 °C for 2 hours and then at room temperature overnight. PEDOT:PSS was filtered with a PVDF filter (0.45 μm) and spin-coated on cleaned (see SI) ITO-coated glass substrate in the air (speed: 3000 rpm / ramp: 5 s / dwelling time: 30 s followed by 5000 rpm / 5 s / 30 s), resulting in a 40 nm thick layer (measured by profilometry). After thermal treatment in the air for 10 minutes at 150 °C, the substrate was quickly transferred in the glovebox. The P3HT:PCBM blend was filtered with a 0.45 μm PVDF filter and spin-coated on top of the PEDOT:PSS layer (1500 rpm / 5 s / 60 s). The

thickness of the P3HT:PCBM layer was estimated by profilometry at 170 ± 10 nm. Annealing was performed at this stage depending on the deposition of the following interfacial layer.

ITO/PEDOT:PSS/P3HT:PCBM/LiF/Al/Ti/MoS₃—The former electrode was annealed at 140 °C for 5 min in the glovebox and 1.2 nm of LiF followed by 100 nm of Al were deposited under vacuum ($< 10^{-6}$ mbar, 0.4 \AA s^{-1} for LiF and 0.15 nm s^{-1} for Al) in a Joule evaporator. 30 to 50 nm of Ti were then evaporated (0.5 \AA s^{-1}). The electrode temperature was close to room temperature and in any case below the annealing temperature used to stabilize the bulk heterojunction. In the glovebox, the MoS₃ solution was spin-coated at 2000 rpm / 5 s / 30 s followed by 20 s at 70 °C to dry the remaining solvent. The thickness of the MoS₃ film was 30 nm (measured by profilometry). ITO/PEDOT:PSS/P3HT:PCBM/Ti/MoS₃ and ITO/PEDOT:PSS/P3HT:PCBM/LiF/Al/MoS₃ were prepared the same way, with only the evaporation of Ti or of LiF/Al respectively. As a reference sample, ITO/PEDOT:PSS/P3HT:PCBM/LiF/Al/Ti/Pt/C photocathodes were made with a Pt/C ink. The ink was prepared by sonicating (1 h) 10 mg of commercial Pt/C (Alfa Aesar, 40 wt.% of Pt, HiSPEC 4000™) in 400 μL of ethanol, 100 μL of deionized water and 65 μL of a Nafion dispersion (D-520, 5 % w/w in water and isopropanol, from Alfa Aesar). The Pt/C ink was spin-coated under the same conditions as the MoS₃ suspension.

ITO/PEDOT:PSS/P3HT:PCBM/C₆₀/MoS₃—P3HT:PCBM deposited on ITO/PEDOT:PSS was annealed at 140 °C for 5 min in the glovebox. C₆₀ (50 nm) was evaporated in a Joule evaporator under vacuum ($< 10^{-6}$ mbar, 0.5 \AA s^{-1} , 500 – 530 °C). The MoS₃ catalytic layer was sprayed on top of the heated (85 °C, cf. SI) solar cell in the air, and the electrode was quickly retransferred into the glovebox.

2.3. Electro- and photo-electrochemical characterization

Electrochemical measurements were recorded using a BioLogic Model VSP 0254 potentiostat. A three-electrode configuration was used. For polarization and electrolysis measurements, a glassy carbon plate and an Ag/AgCl (KCl 3.5 M) electrode were used as the auxiliary electrode and the reference electrode, respectively. Potentials are quoted against the Reversible Hydrogen Electrode. Details of the calibration method for the reference electrode are given in SI.

For the photocatalytic tests, the photocathode was not entirely plunged into the electrolyte (0.5 M H₂SO₄): only the MoS₃ side was put in contact with the electrolyte thanks to a rubber seal with a hole corresponding to the electrochemical area. The glass/ITO side was illuminated with a lamp, as presented in Fig. S1. The samples were illuminated with a 200 W mercury-xenon lamp operated at 106 W coupled with a Spectra-Physics 59472 UV cut-off filter ($\lambda > 440$ nm) and a circular mask. Irradiance at the substrate surface was measured to $\sim 100 \text{ mW cm}^{-2}$ thanks to a Coherent PowerMax-USB PM150-50C Power Sensor.

2.4. Other methods of characterization

The current–voltage characteristics of organic photovoltaic cells were independently measured with a Keithley 2635 system Source Meter under nitrogen atmosphere. They were

deposited onto an ITO-coated substrate with an etched side for the cathodic contact. A LiF/Al cathode (0.28 cm²) was deposited under vacuum in a Joule evaporator (< 10⁻⁶ mbar, 0.4 Å s⁻¹ for 1.2 nm LiF and 0.15 nm s⁻¹ for 100 nm Al). Solar cell performances were characterized under light intensity of AM 1.5 illumination with an Atlas Solar Constant 575PV simulator. The samples were illuminated through the glass substrate.

3. Results and discussion

The effect of interlayers between the MoS₃ catalyst and the P3HT:PCBM BHJ on the photocatalytic performance is investigated by studying the photocurrent and photovoltage of the different photocathodes. They are also compared with the electrocatalytic activity of the bare catalyst, MoS₃, which is an inorganic noble metal-free catalyst for the hydrogen evolution reaction (HER), with 150 mV onset overpotential.²⁶

3.1. Increase of the electronic transfer at the P3HT:PCBM – MoS₃ interface with metallic interlayers

In order to improve the current density previously obtained with ITO/PEDOT:PSS/P3HT:PCBM/MoS₃ in aqueous electrolyte,²⁵ we decided to use a LiF/Al layer intercalated between P3HT:PCBM and MoS₃. LiF/Al is widely used as a cathode material for organic solar cells, as it has a suitable work function which efficiently collects the electrons from the fullerene derivative acceptor. It consists of a thin LiF layer (1.2 nm) and a metallic aluminum layer (typically 100 nm) evaporated under vacuum onto the P3HT:PCBM bulk heterojunction. When such a solar cell is characterized, the voltage is applied between this Al cathode and the ITO anode. The constructions with ITO/PEDOT:PSS/P3HT:PCBM/LiF/Al/MoS₃ architectures did however not exhibit promising properties since the aluminum layer got rapidly oxidized in the acidic electrolyte despite the presence of the spin-coated catalyst overlayer. Such an oxidative process was evidenced by the observation of anodic dark currents, which could not be completely reversed even under illumination (Fig. S2). In other words, the cathodic photocurrent corresponding to H₂ evolution was always found lower than the oxidation dark current. Using a mixed MoS₃:TiO₂ catalyst, as described in our previous work, thicker catalyst films were deposited to achieve better protection of the aluminum layer. In that case, the photocurrent (Fig. S2) (about 0.8 mA cm⁻²) was significantly higher than the dark oxidation current (about 0.2 mA cm⁻²). Nevertheless, the performances were not stable with time and continuous operation resulted in a concomitant decrease of the photocurrent and increase of the dark current as the aluminum layer progressively dissolved in the acidic media.

To protect the Al layer, a metallic titanium layer was evaporated on top of Al. Ti had already been used as a protective layer in a Si-based photocathode.²⁹⁻³² Organic photocathodes with a titanium overlayer were fabricated starting from ITO/PEDOT:PSS/P3HT:PCBM/LiF/Al by depositing a 30 nm thick Ti layer in a Joule evaporator. The voltammogram recorded in 0.5 M H₂SO₄ electrolyte under chopped illumination is presented in Fig. 1, with the J-V curve of the equivalent solar cell for comparison.

The performances of the photoelectrodes were significantly improved compared to our previous devices,²⁵ with a photocurrent value of 8 mA cm⁻² at 0 V vs RHE and reaching 10

mA cm⁻² at more cathodic potentials. The onset of light-driven HER (values were taken at 0.1 mA cm⁻²) was observed at +0.48 V *vs* RHE. Dark HER onset was found at -0.15 V *vs* RHE (black dashed line in Fig. 1), as expected for MoS₃ under these conditions.²⁸ The light-driven anodic shift of the HER onset potential, called photovoltage V_{photo} in the following, was thus found equal to 0.63 V, close to the open-circuit voltage (V_{OC}) of the organic solar cell (approximately 0.6 V). For illuminated photoelectrodes, current limitation occurs at quite negative potentials, which contrasts with the behavior of electrodes based on MoS₃ electrocatalyst alone, which I-V curve continues to increase when decreasing the potential. This plateau (typically 10 mA cm⁻²) thus does not correspond to a diffusion-limited current. It likely originates from saturation of the solar cell as observed in typical current-voltage solar cell characteristics shown in Fig. 1. To verify this hypothesis, the power of the light source was changed. As shown in Fig. 2a, the saturation current changed accordingly. This confirms that the photocurrent value at low potential is limited by the photocurrent produced by the organic solar cell. Moreover, in the range of 0 to 0.5 V, the I-V curve of the photocathode was shifted by approximately 150 mV compared to the solar cell. This value seems to correspond to the overpotential requirement of the MoS₃ catalyst. In order to further investigate this matter of fact, Fig. 2b shows the electro- and photoelectro-chemical HER activity of the unsensitized and OSC-sensitized MoS₃ and Pt/C catalysts. Similarly to MoS₃, the voltammogram of the illuminated ITO/PEDOT:PSS/P3HT:PCBM/LiF/Al/Ti/Pt/C photocathode was anodically shifted by a photovoltage close to the V_{OC} of the solar cell (i.e. approximately 0.6 V) as compared to the voltammogram of the ITO/Pt/C cathode. The difference of onset potentials of both MoS₃ and Pt catalysts was reflected in the difference of onset potentials of the two photocathodes. Fig. 2a and 2b thus shows that both photocurrent and photovoltage are optimal with the LiF/Al/Ti interlayer.

Despite the satisfying performance of the photocathodes, the photo-current decreased under operation (Fig. S3). This was attributed to the fact that the electrolyte could reach the aluminum layer through the Ti layer, resulting in the lift-off of the LiF/Al/Ti/MoS₃ metallic layer, as observed by during the experiment. To avoid this phenomenon, photocathodes were made without the LiF/Al layer.

As shown in Fig. 3, the photocurrent displayed by the photocathode without LiF/Al (blue curve) was similar in intensity to that measured on the photocathode with LiF/Al/Ti. However the HER onset of the new photocathode was 150 mV more negative than the former one containing the LiF/Al layer. Actually the photovoltage provided by the solar cell is limited to 0.45 V (from -0.15 to +0.32 V *vs* RHE), compared to 0.6 V with LiF/Al/Ti. The lower photovoltage obtained without the LiF/Al layer can be attributed to the difference in the metals work functions (Fig. S4), which changes the electron injection barrier.

Stability measurements were then performed with chopped light at 0 V *vs* RHE. The results are presented in Fig. 4. The use of titanium as the sole interfacial layer clearly increased the stability under operation, with a loss of only 12% of the photocurrent over 10 min while the same photocathode with a LiF/Al/Ti interfacial layer was found to lose 45% of its performance under similar conditions (Fig S3). Moreover, after one hour, the titanium layer was not peeled off as the LiF/Al/Ti layer was. Thus, devices made without an aluminum layer were found significantly more stable.

To summarize, the use of metallic layers dramatically increased the efficiencies of the photocathodes compared to the first photocathodes that we reported which displayed photocurrent densities limited to $180 \mu\text{A cm}^{-2}$.²⁵ These interfacial layers bury the P3HT:PCBM layer and electronically separate the catalyst/electrolyte interface and the photovoltaic cell. The p/n junction providing the photovoltage and driving force for HER is therefore not directly related to the difference between the redox potential of interest (H^+/H_2) and the conduction band edge position of the acceptor material (here PCBM). This removes the constraint of their alignment³³ and also explains why the I-V curves obtained with these photocathodes are shaped like the I-V curves of the solar cells: all photogenerated electrons are collected by the metallic layer and then transferred to MoS_3 for catalysis. As no direct liquid-semiconductor junction is formed, these devices can be identified as part of a PV-biased electrosynthetic cell,³⁴ which is bringing the device a step away from the direct sensitization of a catalyst, that is, a step closer to a PV-electrolyzer.⁵ Finding chemically resistant, conductive and water-tight materials is still a challenging task, but metallic titanium is close to meeting all the criteria. Indeed, contrary to aluminum, it does not dissolve in acidic water, and is conductive. However, in terms of photovoltage, the use of a Ti interfacial layer alone shifts the J-V curve 150 mV more negative than with a combined Ti/Al layer. Then, we decided to test a fully organic interfacial layer by evaporating C_{60} , a typical n-type organic semiconductor typically used in OPV cells.

3.2. Organic C_{60} interfacial layer

C_{60} is an organic molecule with a work function located between PCBM and MoS_3 , which makes it suitable as interfacial material for transferring the photogenerated electrons to MoS_3 . Deposition of thin layers is well-controlled with the use of vacuum evaporation. 50 nm of C_{60} were evaporated on P3HT:PCBM and the MoS_3 suspension was then sprayed onto the C_{60} . The voltammogram recorded under chopped light is presented in Fig. 5.

Compared to our first photocathodes (without any interfacial layers, reaching $180 \mu\text{A cm}^{-2}$),²⁵ the saturation photocurrent density and photovoltage are greatly enhanced. The photocurrent for ITO/PEDOT:PSS/P3HT:PCBM/ C_{60} / MoS_3 photocathode is about 1 mA cm^{-2} at 0 V vs RHE (black line in Fig. 5) without any metallic interlayer. Again, the onset potential of the HER is shifted in the anodic direction from -0.15 V vs RHE (MoS_3 in the dark) to $+0.18 \text{ V vs RHE}$ (light-driven HER), i.e. the photosensitizer provides a photovoltage of 0.33 V under operating conditions. The I-V curves of the ITO/PEDOT:PSS/P3HT:PCBM/ C_{60} /LiF/Al solid-state solar cell (Fig. S5) and of the corresponding ITO/PEDOT:PSS/P3HT:PCBM/ C_{60} / MoS_3 photocathode are differing from each other more than the ITO/PEDOT:PSS/P3HT:PCBM/LiF/Al solid-state solar cell and the corresponding ITO/PEDOT:PSS/P3HT:PCBM/LiF/Al/Ti/ MoS_3 photocathode (Fig. 1). Indeed, the current density of the photocathode with C_{60} does not reach the saturation obtained in the corresponding solar cell, while this saturation is reached for the photocathode with the LiF/Al/Ti interfacial layer. This could arise from a higher resistance in electronic transfer from C_{60} to MoS_3 than from Al/Ti to MoS_3 , but also from the fact that the ITO/PEDOT:PSS/P3HT:PCBM/ C_{60} / MoS_3 photocathode does not benefit from the reflectivity of the metallic layer of the ITO/PEDOT:PSS/P3HT:PCBM/LiF/Al/Ti/ MoS_3 photocathode, which enhances the photocurrent density. Moreover, both V_{OC} and J_{SC} of the solid-state ITO/PEDOT:PSS

\P3HT:PCBM\C₆₀\LiF\Al solar cell decreased compared to the ITO\PEDOT:PSS \P3HT:PCBM\LiF\Al solar cell (Fig. S6), possibly because of resistive losses due to the limited C₆₀ conductivity of about 10⁻⁷ S cm⁻¹.³⁵

The hydrophobic nature of C₆₀³⁶ was expected to ensure better stability of the underlying P3HT:PCBM layer by preventing water from reaching it. However Fig. 6 shows that the photocathodes based on C₆₀ interlayers degrade rapidly. The second scan already shows both a decrease of the photocurrent and a shift of the onset HER potential under irradiation towards more negative potentials, finally stabilizing near the equilibrium potential.

These results are consistent with the previous results regarding the effect of a layer burying the P3HT:PCBM BHJ in the whole architecture and suppressing the semi-conductor/ electrolyte interface. During the first cycle, the C₆₀ layer does not contain water and partly separates the P3HT:PCBM material from the electrolyte. In the following cycles, the water progressively diffuses into the C₆₀ layer and progressively reaches the P3HT:PCBM, as if there was no more interfacial layer protecting the device, explaining the shift in the onset HER potential as well as the decrease of photocurrent. The C₆₀ layer increases the photocurrent density at RHE potential to 1 mA cm⁻² without any metallic layer. We are now investigating the possibility of depositing more stable C₆₀ derivatives using wet deposition processes.

In order to further investigate the impact of the interlayer on the photocathode performances we have carefully analyzed the results by means of two figures-of-merit measuring the amount of power saved by the electrode under operation.

3.3. Comparison of the photocathodes performance

The ratiometric power-saved figure-of-merit $\Phi_{\text{saved,ideal}}$ (Equ. (1)) relative to RHE, i.e. an ideally non-polarizable dark electrode for the same reaction, provides information on the ability of a photocathode to achieve hydrogen evolution at potentials more positive than the thermodynamic potential of H⁺/H₂. Unlike the solar-to-hydrogen (STH) efficiency, which applies for devices achieving overall water splitting assayed in a two-electrode configuration^{1,2} (see SI for details), the ratiometric power saved figure-of-merit $\Phi_{\text{saved,ideal}}$ measures the performance of a single photoelectrode tested under illumination in a three-electrode configuration and is extracted from the maximum power point of its current-voltage curve.^{1,2}

$$\Phi_{\text{saved, ideal}} = \eta_F \times \frac{|J_m| \times [E_{\text{light}}(J_m) - E_{\text{RHE}}]}{P_{\text{in}}} = \frac{|J_m| \times E_{\text{light}}^{\text{vsRHE}}(J_m)}{P_{\text{in}}} \quad (1)$$

The potential is referenced to the thermodynamic potential of the half reaction (H⁺/H₂) at the pH of the electrolyte, i.e. referenced to the RHE, and the current density is in mA cm⁻². $\Phi_{\text{saved,ideal}}$ is obtained at the maximum power P_m where the voltage is $E_{\text{light}}(J_m)$ and the current density is J_m (Fig. 7). P_{in} is the power of the incident illumination in mW cm⁻². The Faradaic efficiency η_F for hydrogen evolution is assumed to be 100 %, as reported in the literature.²⁸

Table 1 presents $\Phi_{saved,ideal}$ for the different photocathodes. The current density at 0 V vs RHE and onset potential (arbitrary taken at 0.1 mA cm⁻²) are also presented for comparison between the cells.

First, for identical absorber and interlayer (ITO\PEDOT:PSS\P3HT:PCBM\LiF\Al\Ti) but with two different catalysts (MoS₃ and Pt/C), the $\Phi_{saved,ideal}$ are significantly different, equal to 0.64 % and 1.18 % respectively. This difference mainly comes from the onset potential that is higher with Pt/C (0.67 V) than with MoS₃ (0.48 V, about 200 mV smaller). This is due to the additional overpotential of MoS₃ to catalyze the HER, as shown in Fig. 2b. The short-circuit current is similar with both MoS₃ and Pt/C because the saturation current is reached for both photocathodes at a positive potential, but the current at the maximum power point is slightly higher in the case of the Pt/C catalyst because the saturation current is reached before than in the case of the MoS₃ catalyst. For the ITO\PEDOT:PSS\P3HT:PCBM\Ti\MoS₃ photocathode, $\Phi_{saved,ideal}$ is 0.24 %, i.e. 2.7 times less than with the same catalyst (MoS₃) but different interlayer (LiF\Al\Ti), because the photocatalytic onset potential is closer to 0 V vs RHE (0.32 V), and the saturation current is not reached at a positive potential. Finally, for the C₆₀ interlayer coupled with MoS₃, the onset potential is 0.24 V, close to that with Ti, but the J_0 vs RHE is much lower, probably due to unsatisfactory electronic transfer between C₆₀ and MoS₃, resulting in a slowly increasing HER slope and a small value of $\Phi_{saved,ideal}$ (0.006 %).

$\Phi_{saved,ideal}$ depends on the efficiency of both the photoproduction of charges in P3HT:PCBM and their utilization by the catalyst, which are not differentiated in this figure-of-merit. It may thus be interesting to consider another quantity, which is less catalyst-dependent: the power-saved metric relative to a non-photoactive dark electrode with an identical catalyst and measured in an identical three-electrode electrochemical cell (Fig. 8). $\Phi_{saved,NPAC}$ (NPAC = non-photoactive, identical catalyst) is calculated following equ. (2):¹

$$\begin{aligned}\Phi_{saved,NPAC} &= \eta_F \times \frac{|J_{photo,m}| \times [E_{light}(J_{photo,m}) - E_{dark}(J_{photo,m})]}{P_{in}} \\ &= \eta_F \times \frac{|J_{photo,m}| \times V_{photo,m}}{P_{in}}\end{aligned}\quad (2)$$

where η_F is the Faradaic efficiency assumed to be 100 % again, P_{in} is the power of the incident illumination, and $J_{photo,m}$ and $V_{photo,m}$ are the photocurrent and photovoltage at the maximum power point.

For the comparison of a photoelectrode, $\Phi_{saved,ideal}$ and $\Phi_{saved,NPAC}$ are both important values because $\Phi_{saved,ideal}$ reflects the optimum power point for the use of the photoelectrode in practical applications (i.e. depending on the performance of both the photovoltaic material and the catalyst) while $\Phi_{saved,NPAC}$ reflects the photovoltage and photocurrent of a photocathode independently from the overpotential requirement of the catalyst.

Some details of the procedure to calculate $\Phi_{saved,NPAC}$ are presented in SI. Fig. S7 shows the curves used in the case of the MoS₃ catalyst and the LiF\Al\Ti interfacial layer. The photocurrent J_{photo} is the difference between the current under illumination (J_{light} , i.e.

measured for the ITO\PEDOT:PSS\P3HT:PCBM\LiF\Al\Ti\MoS₃ photocathode) and of the catalyst (J_{dark} , measured for ITO\MoS₃). As expected, J_{photo} increases at the same rate as J_{light} when the voltage is swept in the cathodic direction. Once the onset of the HER of the catalyst is reached, J_{photo} decreases with the increase of J_{dark} . From these data, the photovoltage V_{photo} is obtained by subtracting U_{dark} from U_{light} at matching current densities. J_{photo} as a function of V_{photo} is shown in Fig. S8 (right Y-axis).

Table 2 presents $\Phi_{\text{saved,ideal}}$ and $\Phi_{\text{saved,NPAC}}$ as well as the photovoltages and photocurrents in each case.

First, the $\Phi_{\text{saved,NPAC}}$ and $\Phi_{\text{saved,ideal}}$ for the same system with LiF\Al\Ti as interlayer and MoS₃ as catalyst are significantly different: $\Phi_{\text{saved,NPAC}}$ (2.05 %) is 3.2 times larger than $\Phi_{\text{saved,ideal}}$ (0.64 %). This higher $\Phi_{\text{saved,NPAC}}$ is due to both a higher photovoltage and a higher photocurrent at which the maximum power point is obtained: $V_{\text{photo,m}}$ is 0.41 V while V_{m} is only 0.2 V. This 0.21 V loss is a consequence of the overpotential requirement of the catalyst, and in the photocathode, a significant part of the photovoltage is thus used to overcome the overpotential requirement of MoS₃ to mediate HER. Moreover, the photocurrent $J_{\text{photo,m}}$ (7.8 mA cm⁻²) is 50 % larger than J_{m} (5.1 mA cm⁻²) because the saturation photocurrent is barely reached at positive potentials (towards the RHE). On the contrary, with the Pt/C catalyst (ITO\PEDOT:PSS\P3HT:PCBM\LiF\Al\Ti\Pt/C photocathode), which mediates HER at much lower overpotential values than MoS₃, the difference between the two figures-of-merit is much less: $\Phi_{\text{saved,NPAC}}$ (1.64 %) is only 1.2 times $\Phi_{\text{saved,ideal}}$ (1.42 %), because the photovoltage does not need to be used for overcoming the overpotential of the catalyst (V_{m} and $V_{\text{photo,m}}$ are 0.31 V and 0.39 V respectively).

In a next step, $\Phi_{\text{saved,NPAC}}$ and $\Phi_{\text{saved,ideal}}$ can be compared for two photocathodes with different catalysts (Pt/C and MoS₃) but with identical interfacial layers (LiF\Al\Ti). In this case, $\Phi_{\text{saved,NPAC}}$ with MoS₃ and with Pt (2.05 % and 1.64 %) are closer than the $\Phi_{\text{saved,ideal}}$ (0.64 % and 1.42 %) because the maximum photovoltages in both photocathodes are similar (0.41 V and 0.39 V), as well as the maximum photocurrent densities (7.8 and 6.7 mA cm⁻²). Thus, $\Phi_{\text{saved,NPAC}}$ is independent from the catalyst performance, and is a suitable figure-of-merit for the comparison of different light-harvesting modules. It is illustrated by the ITO \PEDOT:PSS\P3HT:PCBM\Ti\MoS₃ photocathode, whose $\Phi_{\text{saved,NPAC}}$ is 1.3 %, i.e. 1.6 times less than with the LiF\Al\Ti interfacial layer (2.05 %) with identical catalysts (MoS₃). It shows that the lower efficiency obtained with Ti is due to the light-harvesting part and not to the catalyst overpotential requirement. This effect is even more pronounced with the C₆₀ interlayer.

4. Conclusion

Photocathodes based on P3HT:PCBM solar cells and a noble metal-free catalyst, MoS₃, evolve hydrogen at RHE potential thanks to the introduction of interfacial layers, which improved the charge transfer from the photocathode to the catalyst mediating proton reduction. Moreover, these interfacial layers bury the P3HT:PCBM p/n junction, removing

the constraint of energy level alignment between the redox potential of interest (H^+/H_2) and the conduction band edge position of the acceptor material (here PCBM).

The organic cell provides a photovoltage of 0.6 V which is close to the open circuit potential measured in solid state devices when the metallic LiF\Al\Ti layer is used, while the photocurrent at RHE potential reaches 8 mA cm^{-2} , corresponding to a value of ratiometric saved power of 2.05 %. Increased stability is obtained by using only Ti as interfacial layer, though it results in a ratiometric saved power value of 1.30 % due to a 150 mV cathodic shift of the J-V curve. The photovoltage and photocurrent are lower in the case of C_{60} , probably because of resistive losses appearing at the interfaces. As described in a recent work,³⁷ TiO_x layers also works as efficient interfacial layer in this context in combination with Pt as HER catalyst. Using other types of organic and polymeric photovoltaic materials delivering a higher V_{OC} , e.g. PCDTBT (poly[N- 9'-heptadecanyl-2,7-carbazole-alt-5,5-(4,7-di-2-thienyl-2',1',3'-benzothiadiazole)],³⁸ the photovoltage values could be further increased. These promising results show that a rational improvement of the performances of such organic solar cell-based photoelectrodes is possible through the combination of interfacial layers, catalysts and organic semiconductor materials. The stability of the interfacial layers and consequently of the devices must be further improved for their integration into practical application, so that further steps will include the search for novel formulation allowing a more durable protection of the photo-active components against corrosion and integration of multi-junction organic solar cells.

Supplementary Material

Refer to Web version on PubMed Central for supplementary material.

Acknowledgements

We are indebted to the CEA for the financial support, through the DSM Energy Program for the Ph.D. thesis grant assigned to RB. *This work was partially supported by the French National Research Agency (Labex program, ARCANÉ, ANR-11-LABX-0003-01 and the European Research Council under the European Union's Seventh Framework Programme (FP/2007-2013)/ERC Grant Agreement n.306398.*

Notes and references

- (1). Coridan RH, Nielander AC, Francis SA, McDowell MT, Dix V, Chatman SM, Lewis NS. Methods for Comparing the Performance of Energy-Conversion Systems for Use in Solar Fuels and Solar Electricity Generation. *Energy Environ. Sci.* 2015 DOI:10.1039/C5EE00777A.
- (2). Walter MG, Warren EL, McKone JR, Boettcher SW, Mi Q, Santori EA, Lewis NS. Solar Water Splitting Cells. *Chem. Rev.* 2010; 110(11):6446–6473. [PubMed: 21062097]
- (3). Li Z, Luo W, Zhang M, Feng J, Zou Z. Photoelectrochemical Cells for Solar Hydrogen Production: Current State of Promising Photoelectrodes, Methods to Improve Their Properties, and Outlook. *Energy Environ. Sci.* 2013; 6(2):347–370.
- (4). Protti S, Albin A, Serpone N. Photocatalytic Generation of Solar Fuels from the Reduction of H_2O and CO_2 : A Look at the Patent Literature. *Phys. Chem. Chem. Phys.* 2014; 16(37):19790–19827. [PubMed: 25135433]
- (5). Jacobsson TJ, Fjällström V, Edoff M, Edvinsson T. Sustainable Solar Hydrogen Production: From Photoelectrochemical Cells to PV-Electrolyzers and Back Again. *Energy Environ. Sci.* 2014; 7:2056–2070.

- (6). Lanzarini E, Antognazza MR, Biso M, Ansaldo A, Laudato L, Bruno P, Metrangolo P, Resnati G, Ricci D, Lanzani G. Polymer-Based Photocatalytic Hydrogen Generation. *J. Phys. Chem. C*. 2012; 116(20):10944–10949.
- (7). Krebs FC, Hösel M, Corazza M, Roth B, Madsen MV, Gevorgyan SA, Søndergaard RR, Karg D, Jørgensen M. Freely Available OPV - The Fast Way to Progress. *Energy Technol*. 2013; 1(7): 378–381.
- (8). Licht S, Wang B, Mukerji S, Soga T, Umeno M, Tributsch H. Over 18 % Solar Energy Conversion to Generation of Hydrogen Fuel ; Theory and Experiment for Efficient Solar Water Splitting. *Int. J. Hydrogen Energy*. 2001; 26:653–659.
- (9). Rocheleau RE, Miller EL, Misra A. High-Efficiency Photoelectrochemical Hydrogen Production Using Multijunction Amorphous Silicon Photoelectrodes. *Energy Fuels*. 1998; 12(1):3–10.
- (10). Yamada Y, Matsuki N, Ohmori T, Mametsuka H, Kondo M, Matsuda A, Suzuki E. One Chip Photovoltaic Water Electrolysis Device. *Int. J. Hydrogen Energy*. 2003; 28(11):1167–1169.
- (11). Reece SY, Hamel JA, Sung K, Jarvi TD, Esswein AJ, Pijpers JJH, Nocera DG. Wireless Solar Water Splitting Using Silicon-Based Semiconductors and Earth-Abundant Catalysts. *Science*. 2011; 334:645–649. [PubMed: 21960528]
- (12). Morales-Guio CG, Tilley SD, Vrubel H, Grätzel M, Hu X. Hydrogen Evolution from a Copper(I) Oxide Photocathode Coated with an Amorphous Molybdenum Sulphide Catalyst. *Nat. Commun*. 2014; 5:3059. [PubMed: 24402352]
- (13). Lin C-Y, Lai Y-H, Mersch D, Reisner E. Cu₂O/NiO_x Nanocomposite as an Inexpensive Photocathode in Photoelectrochemical Water Splitting. *Chem. Sci*. 2012; 3(12):3482–3487.
- (14). Park Y, McDonald KJ, Choi K-S. Progress in Bismuth Vanadate Photoanodes for Use in Solar Water Oxidation. *Chem. Soc. Rev*. 2013; 42:2321–2337. [PubMed: 23092995]
- (15). Abdi FF, Han L, Smets AHM, Zeman M, Dam B, van de Krol R. Efficient Solar Water Splitting by Enhanced Charge Separation in a Bismuth Vanadate-Silicon Tandem Photoelectrode. *Nat. Commun*. 2013; 4:2195. [PubMed: 23893238]
- (16). Green MA, Emery K, Hishikawa Y, Warta W, Dunlop ED. Solar Cell Efficiency Tables (version 45). *Prog. Photovolt: Res. Appl*. 2015; 23:1–9.
- (17). Li W, Furlan A, Hendriks KH, Wienk MM, Janssen RAJ. Efficient Tandem and Triple-Junction Polymer Solar Cells. *J. Am. Chem. Soc*. 2013; 135(15):5529–5532. [PubMed: 23544881]
- (18). Chen SN, Heeger AJ, Kiss Z, MacDiarmid AG, Gau SC, Peebles DL. Polyacetylene, (CH)_x: Photoelectrochemical Solar Cell. *Appl. Phys. Lett*. 1980; 36(1):96–98.
- (19). Yanagida S, Kabumoto A, Mizumoto K, Pac C, Yoshino K. Poly(p-Phenylene)-Catalysed Photoreduction of Water to Hydrogen. *J. Chem. Soc. Chem. Commun*. 1985:474–475.
- (20). El-Rashiedy OA, Holdcroft S. Photoelectrochemical Properties of Poly (3-Alkylthiophene) Films in Aqueous Solution. *J. Phys. Chem*. 1996; 100:5481–5484.
- (21). Abe T, Nagai K. Novel Photofunctions of Bilayer Composed of P-Type Phthalocyanine and N-Type Organic Semiconductor as Photoelectrodes in the Water Phase. *Org. Electron*. 2007; 8(2-3): 262–271.
- (22). Suppes G, Ballard E, Holdcroft S. Aqueous Photocathode Activity of Regioregular poly(3-Hexylthiophene). *Polym. Chem*. 2013; 4(20):5345–5250.
- (23). Abe T, Tobinai S, Taira N, Chiba J, Itoh T, Nagai K. Molecular Hydrogen Evolution by Organic p/n Bilayer Film of Phthalocyanine/Fullerene in the Entire Visible-Light Energy Region. *J. Phys. Chem. C*. 2011; 115(15):7701–7705.
- (24). Lattach Y, Fortage J, Deronzier A, Moutet J-C. Polypyrrole-Ru(2,2'-bipyridine)₃²⁺/MoS_x Structured Composite Film As a Photocathode for the Hydrogen Evolution Reaction. *ACS Appl. Mater. Interfaces*. 2015; 7(8):4476–4480. [PubMed: 25688728]
- (25). Bourgeteau T, Tondelier D, Geffroy B, Brisse R, Laberty-Robert C, Campidelli S, de Bettignies R, Artero V, Palacin S, Jusselme B. A H₂-Evolving Photocathode Based on Direct Sensitization of MoS₃ with an Organic Photovoltaic Cell. *Energy Environ. Sci*. 2013; 6(9):2706–2713.
- (26). Morales-Guio CG, Hu X. Amorphous Molybdenum Sulfides as Hydrogen Evolution Catalysts. *Acc. Chem. Res*. 2014; 47(8):2671–2681. [PubMed: 25065612]

- (27). Guerrero A, Haro M, Bellani S, Antognazza MR, Meda L, Gimenez S, Bisquert J. Organic Photoelectrochemical Cells with Quantitative Photocarrier Conversion. *Energy Environ. Sci.* 2014; 7(11):3666–3673.
- (28). Vrabel H, Merki D, Hu X. Hydrogen Evolution Catalyzed by MoS₃ and MoS₂ Particles. *Energy Environ. Sci.* 2012; 5(3):6136–6144.
- (29). Seger B, Laursen AB, Vesborg PCK, Pedersen T, Hansen O, Dahl S, Chorkendorff I. Hydrogen Production Using a Molybdenum Sulfide Catalyst on a Titanium-Protected n⁺p-Silicon Photocathode. *Angew. Chem. Int. Ed.* 2012; 51(36):9128–9131.
- (30). Seger B, Pedersen T, Laursen AB, Vesborg PCK, Hansen O, Chorkendorff I. Using TiO₂ as a Conductive Protective Layer for Photocathodic H₂ Evolution. *J. Am. Chem. Soc.* 2013; 135(3):1057–1064. [PubMed: 23289745]
- (31). Seger B, Tilley SD, Pedersen T, Vesborg PCK, Hansen O, Grätzel M, Chorkendorff I. Silicon Protected with Atomic Layer Deposited TiO₂: Conducting versus Tunnelling through TiO₂. *J. Mater. Chem. A.* 2013; 1(47):15089–15094.
- (32). Seger B, Tilley DS, Pedersen T, Vesborg PCK, Hansen O, Grätzel M, Chorkendorff I. Silicon Protected with Atomic Layer Deposited TiO₂: Durability Studies of Photocathodic H₂ Evolution. *RSC Adv.* 2013; 3(48):25902–25907.
- (33). Jacobsson TJ, Fjällström V, Sahlberg M, Edoff M, Edvinsson T. A Monolithic Device for Solar Water Splitting Based on Series Interconnected Thin Film Absorbers Reaching over 10% Solar-to-Hydrogen Efficiency. *Energy Environ. Sci.* 2013; 6(12):3676–3683.
- (34). Nielander AC, Shaner MR, Papadantonakis KM, Francis SA, Lewis NS. A Taxonomy for Solar Fuels Generators. *Energy Environ. Sci.* 2015; 8(1):16–25.
- (35). Rikitake K, Akiyama T, Takashima W, Kaneto K. Relationships between Crystallinity and Conductivity in Evaporated C₆₀ Films. *Synth. Met.* 1997; 86:2357–2358.
- (36). Labille J, Brant J, Villiéras F, Pelletier M, Thill A, Masion A, Wiesner M, Rose J, Bottero J-Y. Affinity of C₆₀ Fullerenes with Water. *Fullerenes, Nanotubes, Carbon Nanostruct.* 2006; 14(2-3):307–314.
- (37). Haro M, Solis C, Molina G, Otero L, Bisquert J, Gimenez S, Guerrero A. Towards Stable Solar Hydrogen Generation Using Organic Photoelectrochemical Cells. *J. Phys. Chem. C.* 2015; 119(12):6488–6494.
- (38). Park SH, Roy A, Beaupré S, Cho S, Coates N, Moon JS, Moses D, Leclerc M, Lee K, Heeger AJ. Bulk Heterojunction Solar Cells with Internal Quantum Efficiency Approaching 100%. *Nat. Photonics.* 2009; 3(5):297–302.

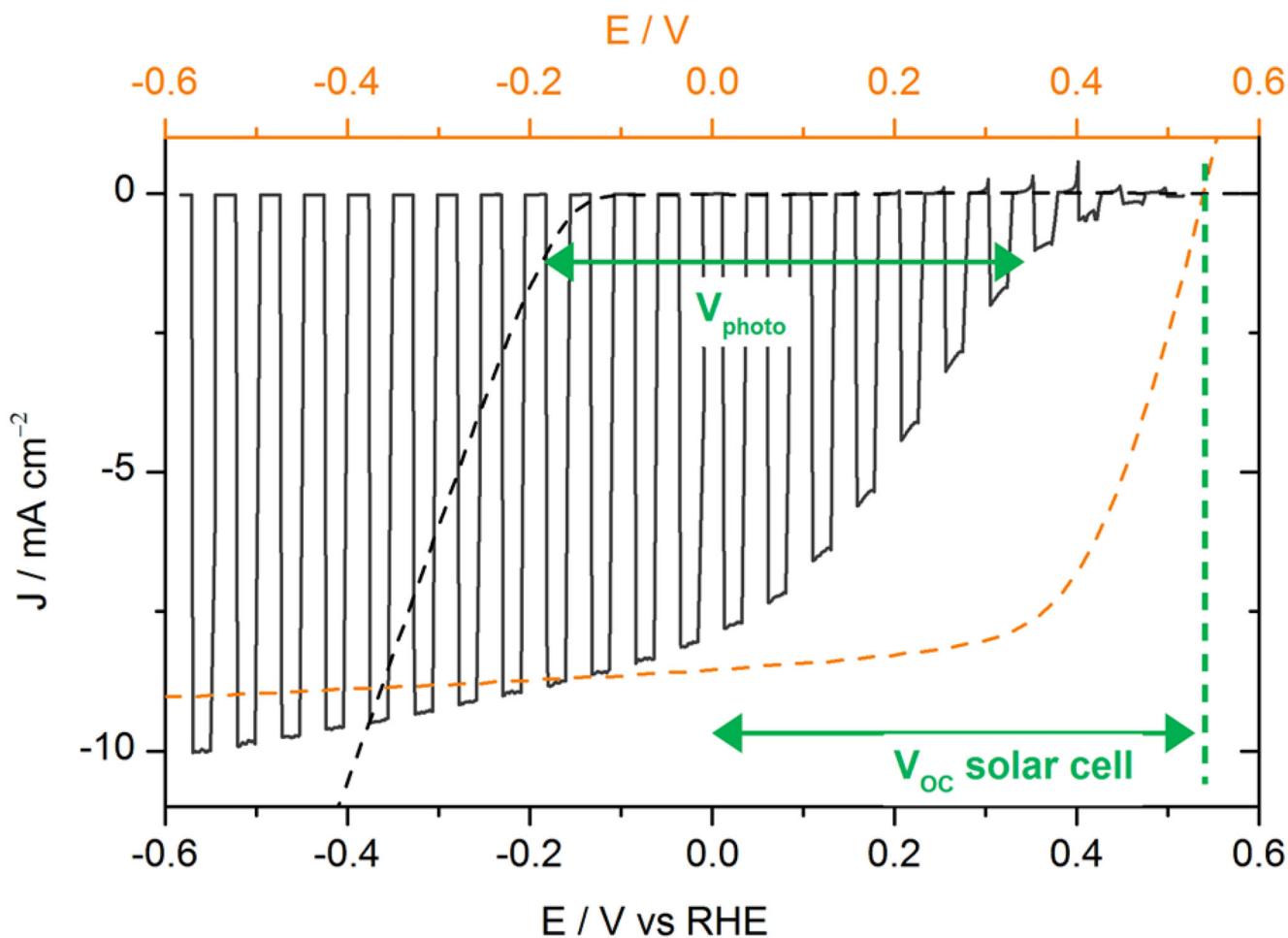


Figure 1.

Voltammogram recorded at 50 mV s^{-1} in $0.5 \text{ M H}_2\text{SO}_4$ with chopped visible light for an ITO/PEDOT:PSS/P3HT:PCBM/LiF/Al/Ti/MoS₃ photocathode (black line, electrode area 0.32 cm^2), and recorded at 5 mV s^{-1} in $0.5 \text{ M H}_2\text{SO}_4$ for an ITO/MoS₃ cathode (black dashed line, electrode area 0.28 cm^2). Potentials are referred to the RHE (bottom axis). The current-voltage curve of an ITO/PEDOT:PSS/P3HT:PCBM/LiF/Al solar cell (orange dashed line, top axis) is shown for comparison.

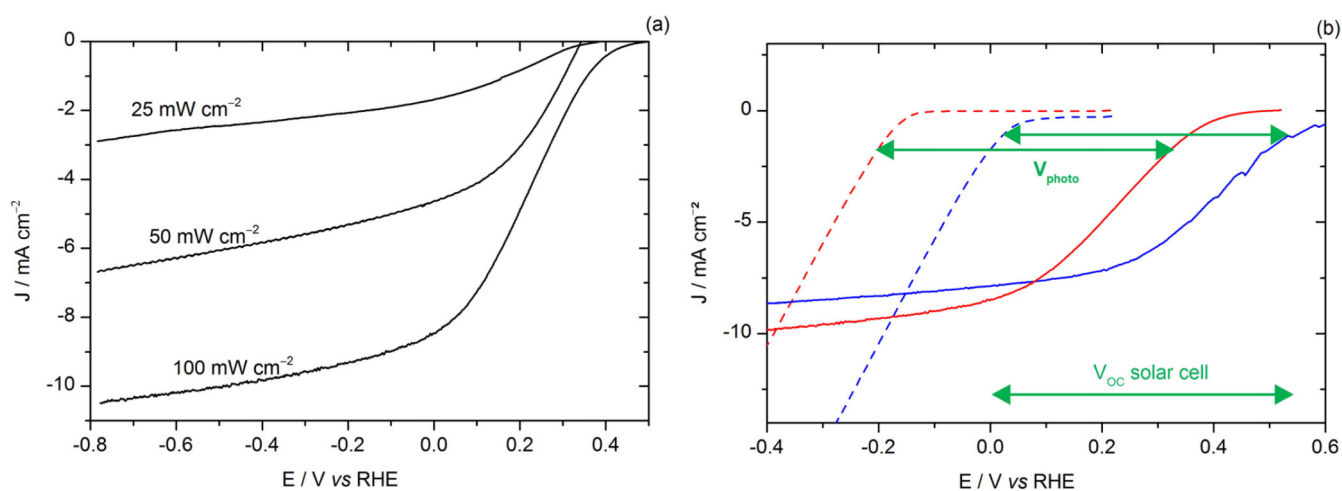


Figure. 2.

(a) Voltammograms recorded at 50 mV s^{-1} in $0.5 \text{ M H}_2\text{SO}_4$ with visible light illumination for a ITO/PEDOT:PSS/P3HT:PCBM/LiF/Al/Ti/MoS₃ photocathode. The power of the light source was changed from $\sim 100 \text{ mW cm}^{-2}$ to $\sim 25 \text{ mW cm}^{-2}$. New photocathodes were taken for each test with a different power. Electrode area: 0.32 cm^2 . (b) Voltammogram recorded at 5 mV s^{-1} in $0.5 \text{ M H}_2\text{SO}_4$ for an ITO/MoS₃ cathode (red dotted line) and an ITO/Pt/C cathode (blue dotted line) and at 50 mV s^{-1} with visible light illumination (100 mW cm^{-2}) for an ITO/PEDOT:PSS/P3HT:PCBM/LiF/Al/Ti/MoS₃ photocathode (red line), and an ITO/PEDOT:PSS/P3HT:PCBM/LiF/Al/Ti/Pt/C photocathode (blue line).

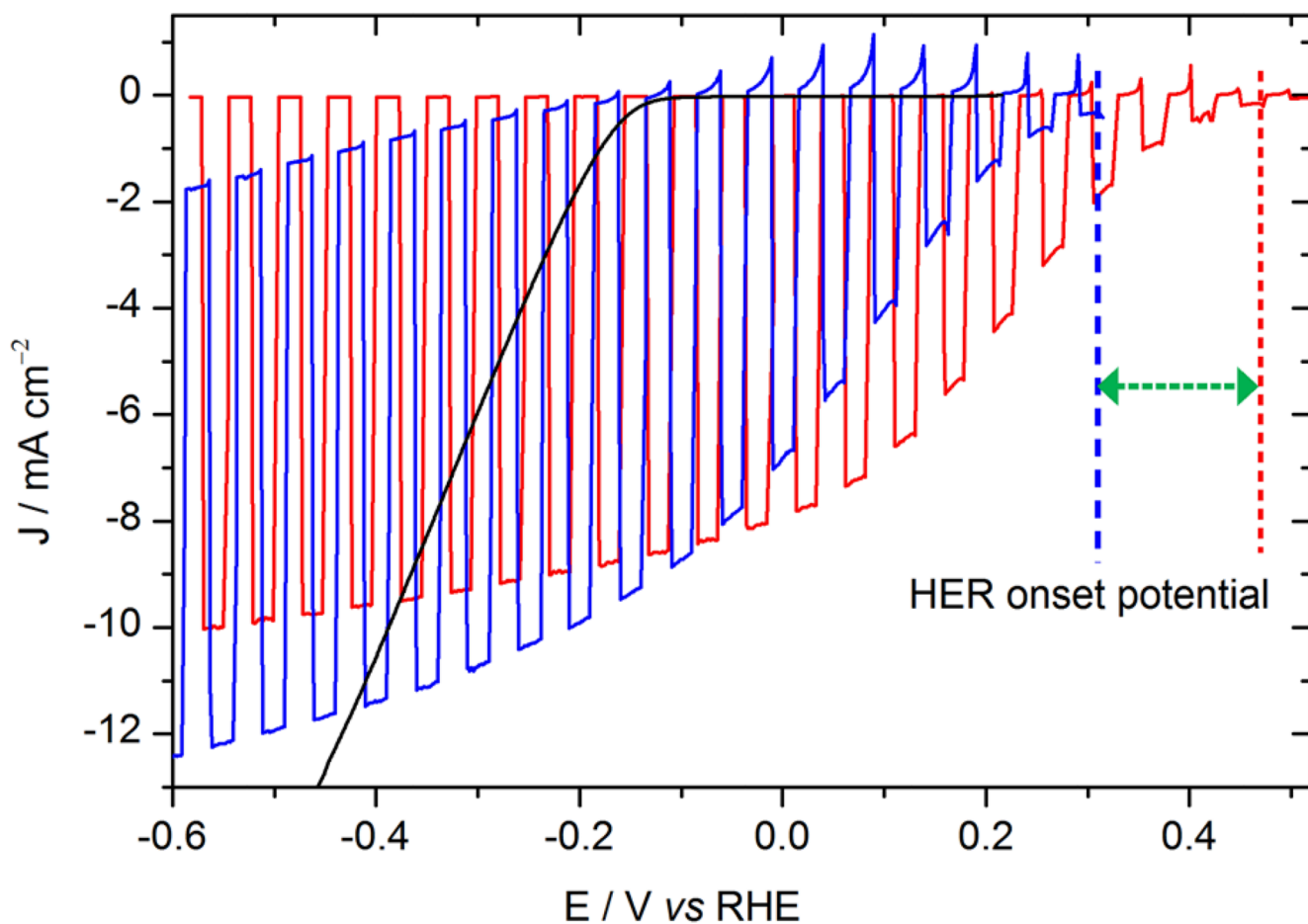


Figure 3. Voltammograms recorded at 50 mV s^{-1} in $0.5 \text{ M H}_2\text{SO}_4$ with chopped visible light. Red: ITO/PEDOT:PSS/P3HT:PCBM/LiF/Al/Ti/MoS₃ photocathode (electrode area: 0.32 cm^2); blue: ITO/PEDOT:PSS/P3HT:PCBM/Ti/MoS₃ (0.28 cm^2). The green arrow represents the shift of the HER onset potential of 150 mV .

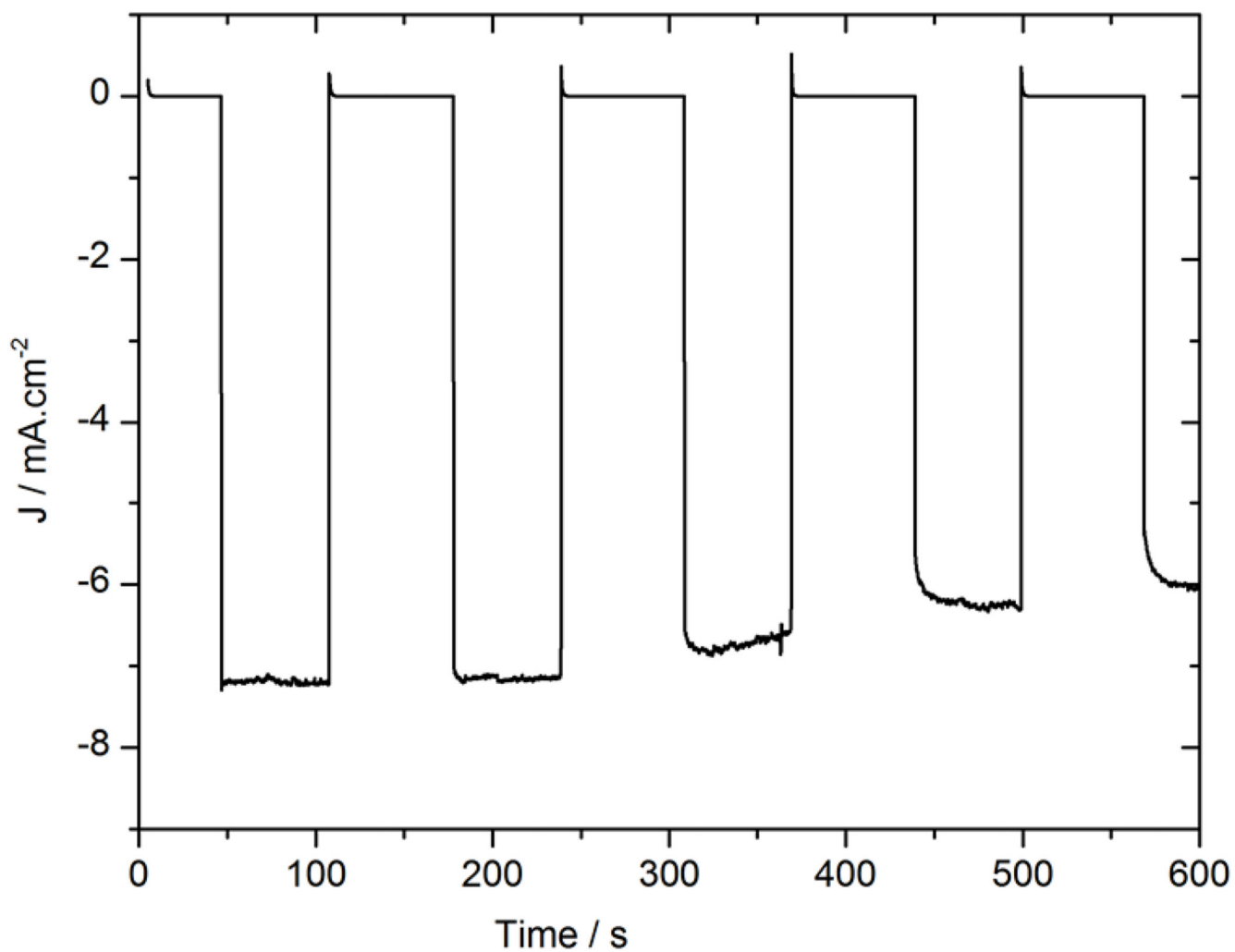


Figure. 4. Chronoamperometry at 0 V *vs* RHE in 0.5 M H₂SO₄ with chopped visible light for an ITO \PEDOT:PSS\P3HT:PCBM\Ti\MoS₃ photocathode (black). Electrode area: 0.28 cm².

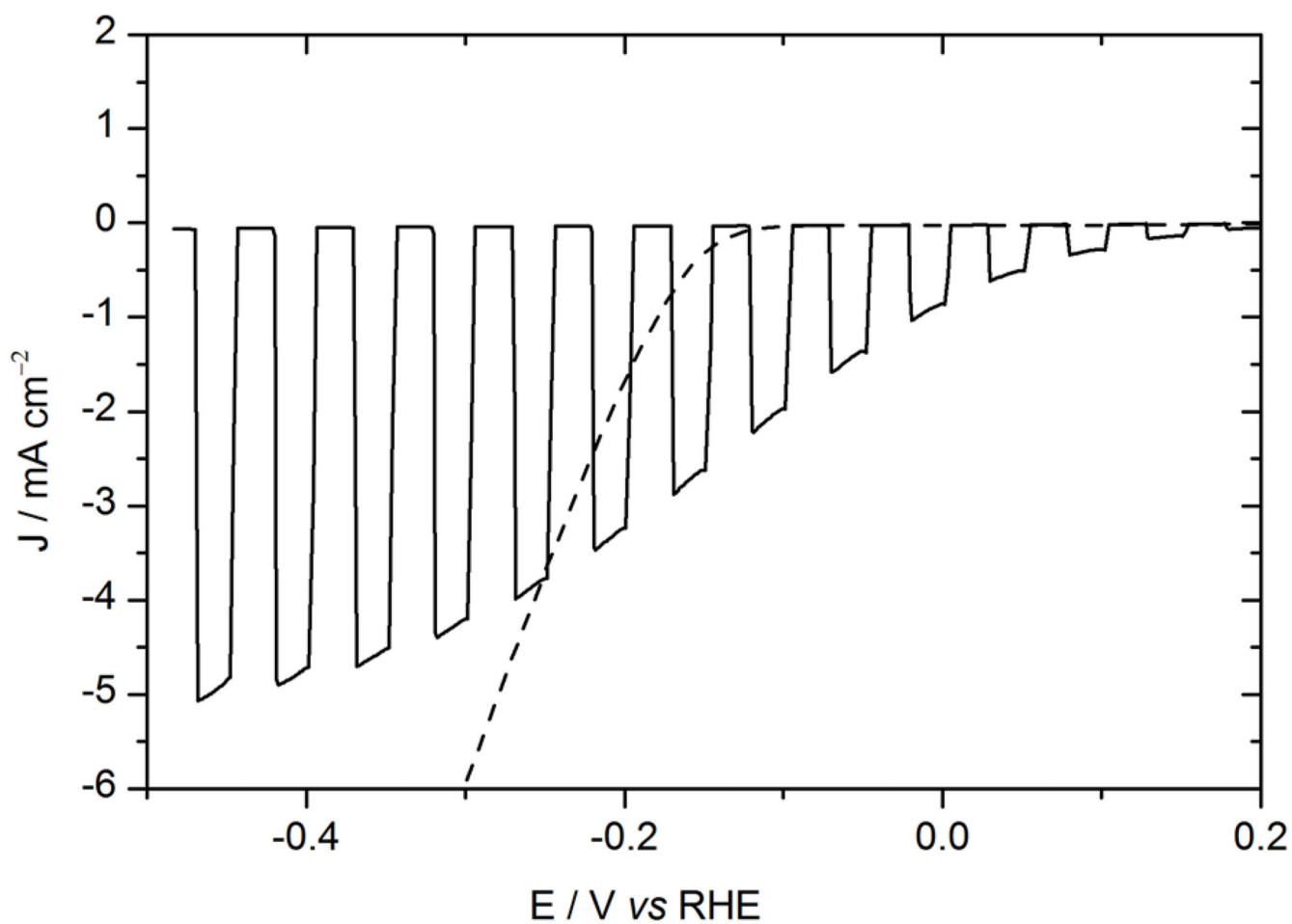


Figure. 5. Voltammogram recorded at 50 mV s^{-1} in $0.5 \text{ M H}_2\text{SO}_4$ with chopped visible light for an ITO/PEDOT:PSS/P3HT:PCBM/C₆₀/MoS₃ photocathode (electrode area: 0.06 cm^2). The polarization curve of ITO/MoS₃ recorded at 5 mV s^{-1} is shown for comparison (dashed line, electrode area: 0.28 cm^2).

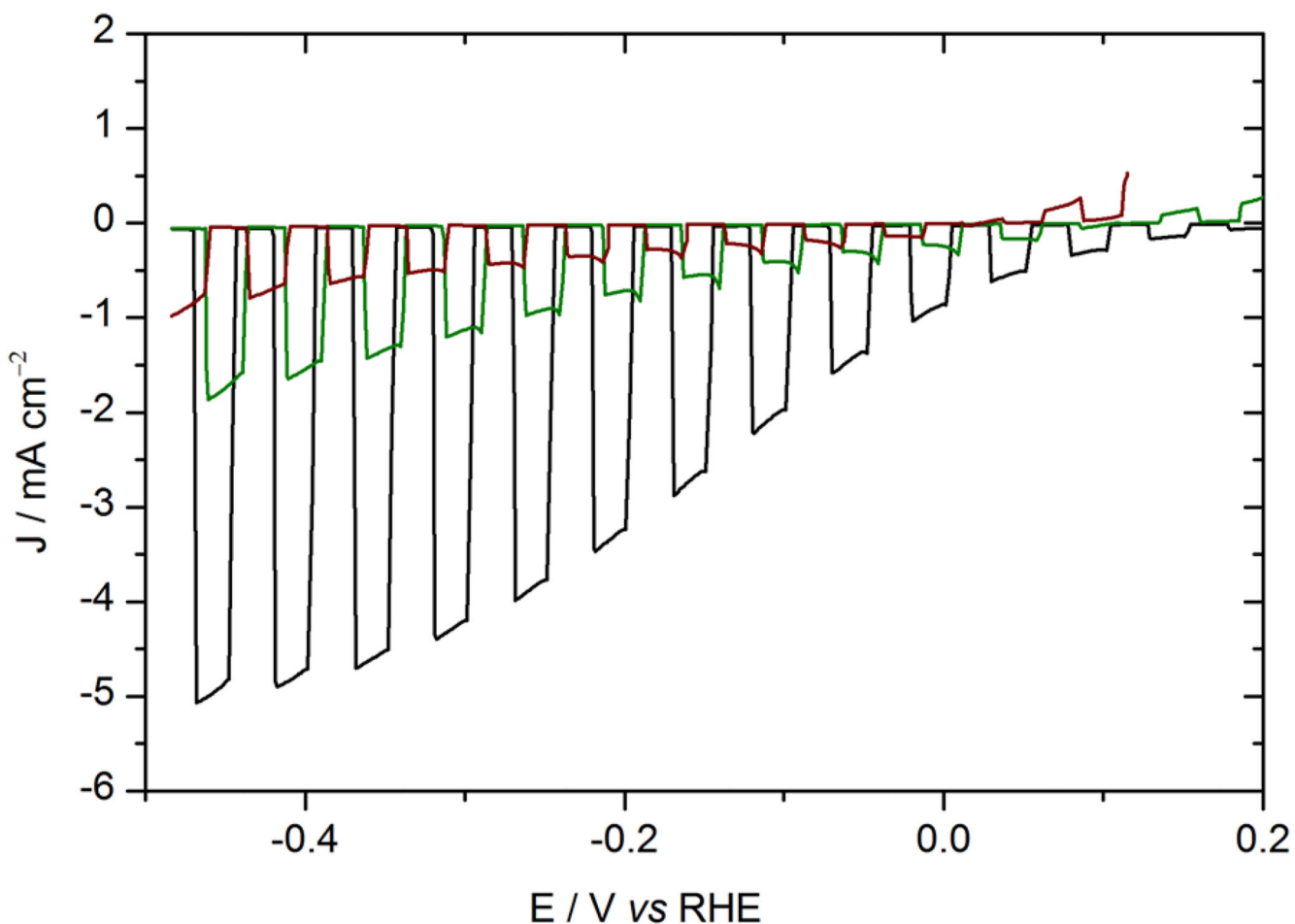


Figure 6.

Voltammograms recorded at 50 mV s^{-1} in $0.5 \text{ M H}_2\text{SO}_4$ with chopped visible light for the same ITO/PEDOT:PSS/P3HT:PCBM/C₆₀/MoS₃ photocathode. Black: 1st cycle (same as Fig. 5); green: 2nd cycle; brown: 3rd cycle. Electrode area: 0.06 cm^2 . The oxidation current appearing at anodic potentials was also appearing in configurations without C₆₀; thus, the oxidation current was not attributed to a possible reaction or degradation of C₆₀ but more probably to the absence of equilibration time between the measurements.

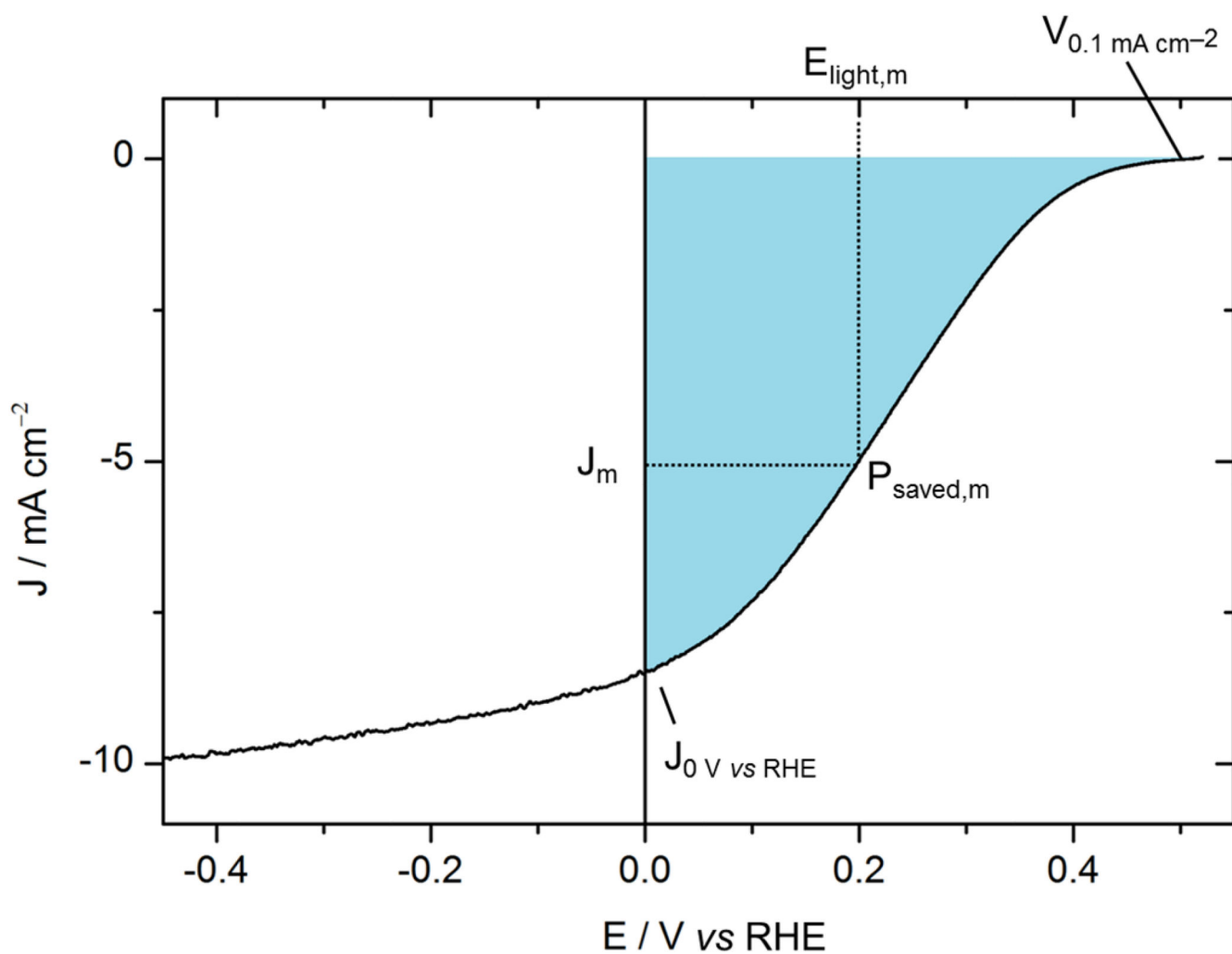


Figure. 7. Current-voltage characteristic of an ITO/PEDOT:PSS/P3HT:PCBM/LiF/Al/Ti/MoS₃ photocathode (black line).

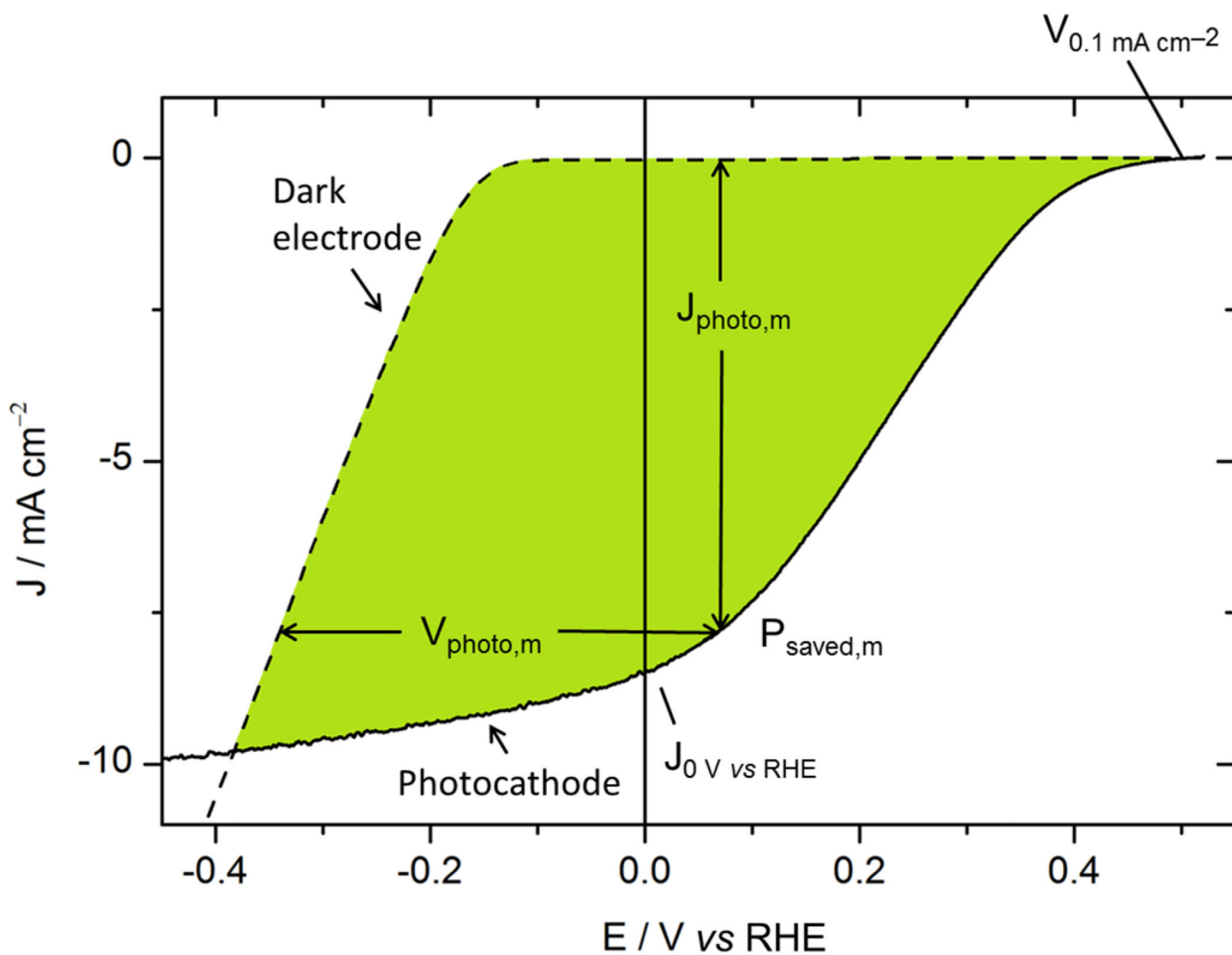


Figure 8.

Current-voltage characteristic of an ITO/PEDOT:PSS/P3HT:PCBM/LiF/Al/Ti/MoS₃ photocathode (black line) and of an ITO/MoS₃ dark cathode (black dashed line). The photovoltage at a given current is thus evaluated from the potential under illumination compared to that of the same catalyst directly deposited on ITO.

Table 1

J_0 *V vs RHE*, $V_{0.1 \text{ mA cm}^{-2}}$ and $\Phi_{\text{saved,ideal}}$ of the different photocathodes. $V_{0.1 \text{ mA cm}^{-2}}$, the onset potential, is the voltage necessary to obtain a current density that was arbitrary chosen at 0.1 mA cm^{-2} , and J_0 *V vs RHE* is the current density obtained at the thermodynamic potential. Two different areas were taken into account for $\Phi_{\text{saved,ideal}}$ calculation: the current density J_{mp} was multiplied by the electrode area in contact with the electrolyte, while P_{in} was referred to the lightened area (0.5 cm^2), as this area would collect the electrons and transport them to the electrochemical area. If no distinction is made between these two areas, it results in an overestimation of the $\Phi_{\text{saved,ideal}}$ value (1.00 %, 0.432 %, 1.84 % and 0.03 % respectively).

	$V_{0.1 \text{ mA cm}^{-2}}$ / V	J_0 <i>V vs RHE</i> / mA cm^{-2}	$\Phi_{\text{saved,ideal}}$
ITO/PEDOT:PSS/P3HT:PCBM/LiF/Al/Ti/MoS ₃	0.48	8.47	0.641 %
ITO/PEDOT:PSS/P3HT:PCBM/LiF/Al/Ti/Pt/C	0.67	7.87	1.18 %
ITO/PEDOT:PSS/P3HT:PCBM/Ti/MoS ₃	0.32	6.81	0.241 %
ITO/PEDOT:PSS/P3HT:PCBM/C ₆₀ /MoS ₃	0.24	0.86	0.006 %

Table 2

For different photocathodes measured at 100 mW cm^{-2} : $\Phi_{saved,ideal}$ and $\Phi_{saved,NPAC}$ at maximum power point with their corresponding current density and potential (J_{mp} and V_{mp} , $J_{photo,mp}$ and $V_{photo,mp}$). Table S1 gathers all data of Tables 1 and 2, as well as the calculation for the ITO/PEDOT:PSS/P3HT:PCBM/LiF/Al/Ti/MoS₃ at different incident power. As for Table 1, two different areas were taken into account: the current density $J_{photo,mp}$ was multiplied by the electrode area in contact with the electrolyte, while P_{in} was referred to the lightened area (0.5 cm^2).

	$\Phi_{saved,ideal}$	$\Phi_{saved,NPAC}$
ITO/PEDOT:PSS/P3HT:PCBM/LiF/Al/Ti/MoS ₃	0.64 % ($J_m = 5.1 \text{ mA cm}^{-2}$, $V_m = 0.20 \text{ V}$)	2.05 % ($J_{photo,m} = 7.8 \text{ mA cm}^{-2}$, $V_{photo,m} = 0.41 \text{ V}$)
ITO/PEDOT:PSS/P3HT:PCBM/LiF/Al/Ti/Pt/C	1.42 % ($J_m = 6.0 \text{ mA cm}^{-2}$, $V_m = 0.31 \text{ V}$)	1.64 % ($J_{photo,m} = 6.7 \text{ mA cm}^{-2}$, $V_{photo,m} = 0.39 \text{ V}$)
ITO/PEDOT:PSS/P3HT:PCBM/Ti/MoS ₃	0.24 % ($J_m = 3.9 \text{ mA cm}^{-2}$, $V_m = 0.11 \text{ V}$)	1.30 % ($J_{photo,m} = 7.7 \text{ mA cm}^{-2}$, $V_{photo,m} = 0.30 \text{ V}$)
ITO/PEDOT:PSS/P3HT:PCBM/C ₆₀ /MoS ₃	0.006 % ($J_m = 0.4 \text{ mA cm}^{-2}$, $V_m = 0.008 \text{ V}$)	0.14 % ($J_{photo,m} = 2.1 \text{ mA cm}^{-2}$, $V_{photo,m} = 0.30 \text{ V}$)